UNSYS digital

Journal of Unmanned System Technology

Static Output Feedback Control for an Integrated Guidance and Control of a Micro Air Vehicle

K Harikumar, Joseph Arun, M Seetharama Bhat, and S N Omkar

Indian Institute of Science, Bangalore, India

***Abstract*—**In this paper, a static output feedback controller is designed for a 150 mm fixed wing micro air vehicle (MAV). Due to the strong coupling between the longitudinal and lateral dynamics, a static output feedback (SOF) controller is designed using a combined novel eight state dynamic model. The design is carried out in a digital domain which helps in practical implementation of the proposed controller. A blend of classical H_∞ robust control and evolutionary algorithm (genetic algorithm) is used to obtain the static output feedback gains. The proposed controller is also designed under a novel twelve state integrated guidance and control framework.

***Keywords*—** Micro air vehicles, static output feedback, integrated guidance and control.

I. INTRODUCTION

Micro air vehicles (MAV) have typical wing span of less than 300 mm and are used for short range surveillance applications. Navigation and control of such vehicles are difficult due to their small size and large disturbances as compared to their inertial and control forces. For such vehicles, the controller should be robust against disturbances and uncertainties. Owing to the limited computational power available in the onboard computer, the guidance and control algorithm should be simple enough to be implemented. Development of a fixed structure output feedback flight control law by combining the flight qualities criterion with robustness to structured and unstructured uncertainties in design specification is explained in [1]. In references [2]-[5] implement a static output feedback (SOF) control law for an unmanned air vehicle where the H_∞ loop shaping design procedure is utilized and the controller is designed based on the solution of a single Algebraic Riccati Equation (ARE) and two algebraic matrix equations. Incorporation of multiobjective constraints in a static output feedback formulation results in a bilinear matrix inequality (BMI). BMI can be solved using the hybrid approach of combining linear matrix inequalities (LMI) with search methods like Salomon's evolutionary gradient search (EGS) method, as in [6]. A method of tuning robust static output feedback (SOF) controllers in the presence of multiple plant parametric uncertainties using Kharitonov's theorem and evolutionary algorithms is explained in [7]. H_∞ static output feedback control is designed by combining particle swarm optimization, differential evolution and linear matrix inequalities (LMI) [8]. A single robust controller has to satisfy the control system design requirements to avoid gain scheduling while keeping in mind a small flight envelope of MAV. ν-Gap metric analysis [9] is applied to identify the nominal plant model for robust control design. A discrete time H_∞ output feedback controller is designed for a thrust vectored aircraft in [10]. Strengthened discrete optimal projection equations are solved to obtain a fixed order H_2 controller for stabilizing a micro air vehicle in [11]. A modified Iterative Linear Matrix Inequality (ILMI) algorithm is used for the lateral control of a 300 mm MAV in [12].

In this paper, a novel approach to MAV control design is proposed where the coupling between the longitudinal and lateral dynamics is taken into account. Unlike in bigger aircraft, the coupling between the longitudinal and lateral dynamics is significant in MAVs due to their low inertia and higher turning rates. Section II explains the coupling between longitudinal and lateral dynamics of 150 mm MAV. A single controller is designed for the entire flight envelope. So the controller should be robust against change in operating conditions and unmodelled dynamics. Section III deals with the control system design specifications and the selection of nominal model for control design. The controller is synthesized in a multivariable framework unlike in a conventional successive loop closure method where the entire control design is performed for each single input single output (SISO) loop. H_∞ control formulation allows multivariable control design with the required performance and robustness and is explained in SectionIV. With the limited computational power available in the onboard hardware of MAVs, fixed structure controller is a favorable solution for practical implementation. A static output feedback controller designed here meets the closed loop control system specifications. In Section V, an algorithm for obtaining static output feedback gain for the combined longitudinal and lateral state space model is explained. This algorithm uses a combination of LMI and genetic algorithm to obtain the gains in discrete time domain. Section VI deals with integrated guidance and control. Integrated guidance and control removes the requirement of bandwidth separation between the guidance loop and control loop as in separate guidance and control system design. It also avoids the retuning of guidance loop to maintain the stability of the combined system. Simulation results are presented in Section VII.

II. DYNAMIC MODEL OF KH2013A MAV

The MAV KH2013A is shown in **Figure 1**. It has a rectangular wing of 150 mm span. KH2013A is a flying wing MAV, with modified E387 airfoil of thickness 25 %. It has two winglets to improve lateral stability and also to reduce induced

Corresponding author: K Harikumar (e-mail: harikumar@aero.iisc.ernet.in).
This paper was submitted on November 29, 2013; revised on March 05, 2014; and accepted on May 14, 2014.

drag. It has two control surfaces, elevator and rudder. Elevons are not used since they induce a strong coupling between rolling and pitching motions. The physical parameters of the MAV are given in **TABLE I**. In **TABLE I**, J_{xx}, J_{yy} ,J_{zz} are the moment of inertia along the MAV body axis X, Y, Z respectively and J_{xz} is the product of inertia term. Nonlinear dynamics of the MAV are given in (1) to (12) [13].

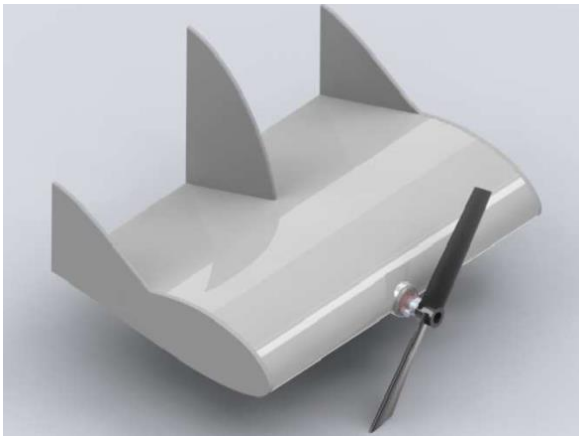

Figure 1 SOLIDWORKS model of KH2013A MA

TABLE I
Physical parameters of KH2013A

Planform	Rectangular
Airfoil	Modified E387
Weight	44 grams
Velocity	9-19 m/s
Reynolds number	60000-130000
Chord	0.11 m
Span	0.15 m
Area	0.0165 m^2
J_{xx}	13.095 x 10^{-6} kg·m^2
J_{yy}	29.348 x 10^{-6} kg·m^2
J_{zz}	39.803 x 10^{-6} kg·m^2
J_{xz}	1.905 x 10^{-6} kg·m^2

In the non-linear equations of motion, (u, v, w) are the component of the velocity of the MAV measured along the body XYZ axis, (p, q, r) are the roll rate, pitch rate and yaw rate respectively measured along the body XYZ axis. The triple (φ, θ, ψ) are the Euler angles and (x, y, z) are the position of the MAV in the inertial frame. (X_a, Y_a, Z_a) are the aerodynamic forces and (L, M, N) represents the moments along the body XYZ axis. T_h is the thrust input, g is the acceleration due to gravity and m is the mass of the MAV. The positive inertial X axis is towards north, positive inertial Y axis is towards east and positive inertial Z axis is towards down as per the convention used in flight dynamics [14]. In equations (1) to (12), and subsequently, cθ represents cosθ, sθ represents sinθ and tθ represents tanθ.

$$\dot{u} = rv - qw - gs\theta + \frac{X_a}{m} + \frac{T_h}{m} \quad (1)$$

$$\dot{v} = pw - ru - g\,s\phi\,c\theta + \frac{Y_a}{m} \quad (2)$$

$$\dot{w} = qu - pv + g\,c\phi\,c\theta + \frac{Z_a}{m} \quad (3)$$

$$\dot{p} = t_1 pq - t_2 qr + t_3 L + t_4 N \quad (4)$$

$$\dot{q} = t_5 pr + t_6(r^2 - p^2) + \frac{M}{J_{yy}} \quad (5)$$

$$\dot{r} = t_7 pq - t_1 qr + t_4 L + t_8 N \quad (6)$$

$$\dot{\phi} = p + q\,s\phi\,t\theta + r\,c\phi s\theta \quad (7)$$

$$\dot{\theta} = q\,c\phi - rs\phi \quad (8)$$

$$\dot{\Psi} = q\,s\phi sec\theta + rc\phi\,sec\theta \quad (9)$$

$$\dot{x} = (c\,\theta c\Psi)u + (s\phi s\theta c\Psi - c\phi s\Psi)v + (c\phi s\theta c\Psi + s\phi s\Psi)w \quad (10)$$

$$\dot{y} = (c\,\theta s\Psi)u + (s\phi s\theta s\Psi + c\phi c\Psi) + (c\phi s\theta s\Psi - s\phi c\Psi)w \quad (11)$$

$$\dot{z} = -(s\theta)u + (s\phi c\theta)w + (c\phi c\theta)w \quad (12)$$

where

$$\Gamma = J_{XX}J_{ZZ} - J_{XZ}J_{XZ} \quad (13)$$

$$t_1 = \frac{J_{XZ}(J_{XX} - J_{YY} + J_{ZZ})}{\Gamma} \quad (14)$$

$$t_2 = \frac{(J_{ZZ}(J_{ZZ} - J_{YY}) + J_{XZ}J_{XZ})}{\Gamma} \quad (15)$$

$$t_3 = \frac{J_{ZZ}}{\Gamma} \quad (16)$$

$$t_4 = \frac{J_{XZ}}{\Gamma} \quad (17)$$

$$t_5 = \frac{J_{ZZ} - J_{XX}}{J_{YY}} \quad (18)$$

$$t_6 = \frac{J_{XZ}}{J_{YY}} \quad (19)$$

$$t_7 = \frac{(J_{XX}(J_{XX} - J_{YY}) + J_{XZ}J_{XZ})}{\Gamma} \quad (20)$$

$$t_8 = \frac{J_{XX}}{\Gamma} \quad (21)$$

The details of the static derivatives, dynamic derivatives and control derivatives for the MAV can be found in [13]. For MAVs, the coupling between the longitudinal and lateral dynamics is strong due to its small rolling inertia and high turn rates. The combined linear state space model can be obtained as given in (22).

$$\begin{Bmatrix} \dot{X_{long}} \\ \dot{X_{lat}} \end{Bmatrix} = \begin{bmatrix} A_{long} & A_{longlat} \\ A_{latlong} & A_{lat} \end{bmatrix} \begin{Bmatrix} X_{long} \\ X_{lat} \end{Bmatrix} + \begin{bmatrix} B_{long} \\ B_{lat} \end{bmatrix} \begin{bmatrix} \delta_e \\ \delta_r \\ \delta_{Th} \end{bmatrix} \quad (22)$$

where

$$X_{long} = [\tilde{u}, \tilde{w}, \tilde{q}, \tilde{\theta}]^T$$
$$X_{lat} = [\tilde{v}, \tilde{p}, \tilde{r}, \tilde{\phi}]^T \quad (23)$$

$$A_{long} = \begin{bmatrix} X_u & X_w & X_q & -gc\theta \\ Z_u & Z_w & Z_q & -gs\theta c\phi \\ M_u & M_w & M_q & 0 \\ 0 & 0 & c\phi & 0 \end{bmatrix} \quad (24)$$

$$A_{lat} = \begin{bmatrix} Y_v & Y_p & Y_r & gc\theta c\phi \\ L_v & L_p & L_r & 0 \\ N_v & N_p & N_r & 0 \\ 0 & 1 & t\theta c\phi & qt\theta c\phi - rt\theta s\phi \end{bmatrix} \quad (25)$$

$$A_{longlat} = \begin{bmatrix} X_v & 0 & v & 0 \\ Z_v & -v & 0 & -gc\theta s\phi \\ M_v & t_5 r - 2t_6 p & t_5 p + 2t_6 r & 0 \\ 0 & 0 & -s\phi & -qs\phi - rc\phi \end{bmatrix} \quad (26)$$

$$A_{latlong} = \begin{bmatrix} Y_u & Y_w & 0 & -gs\theta s\phi \\ L_u & L_w & t_1 p - t_2 r & 0 \\ N_u & N_w & t_7 p - t_1 r & 0 \\ 0 & 0 & t\theta s\phi & \frac{qs\phi + rc\phi}{(c\theta)^2} \end{bmatrix} \quad (27)$$

$$B_{long} = \begin{bmatrix} X_{\delta_e} & 0 & X_{\delta_{Th}} \\ Z_{\delta_e} & 0 & 0 \\ M_{\delta_e} & 0 & 0 \\ 0 & 0 & 0 \end{bmatrix} \quad (28)$$

$$B_{lat} = \begin{bmatrix} 0 & Y_{\delta_r} & 0 \\ 0 & L_{\delta_r} & 0 \\ 0 & N_{\delta_r} & 0 \\ 0 & 0 & 0 \end{bmatrix} \quad (29)$$

For an unmanned aircraft, the important steady flight conditions are the straight and level flight, constant altitude turn and turn with a constant climb rate. In all three flight conditions, the airspeed is assumed to be constant. Coupling between the longitudinal and lateral dynamics happens, in most likelihood, in the turning flight or at high angle of attack flight condition [15]. The nonlinear equations from (1) to (8) and (12) are solved to obtain trim conditions corresponding to a steady turn with constant altitude and steady turn with constant climb condition. The airspeed is selected as 12 m/s and the turn rate is varied from 0 rad/s to 0.8 rad/s. In **Figure 2** and **Figure 3**, the longitudinal modes for steady turn flight conditions for the coupled and decoupled model are shown. Similarly, the lateral modes are shown in **Figure 4** and **Figure 7**. For steady turn with climb conditions, the turn rate is held at 0.6 rad/s and the climb rate is varied from 0 to 2 m/s. The longitudinal modes for steady turn with climb flight conditions for the coupled and decoupled model are shown in **Figure 5** and **Figure 8**. In **Figure 6** and **Figure 9**, the lateral modes are shown. From the **Figure 2** to **Figure 9**, the main inferences obtained are

1) Short period frequency and damping ratio is hardly affected by the coupling terms.
2) The coupled model shows higher phugoid frequency and lower damping ratio when compared to the decoupled model.
3) Roll subsidence mode is nearly the same in both coupled and uncoupled models.
4) Dutch roll mode is having higher frequency and lower damping ratio for the coupled model when compared to the decoupled model.
5) The spiral mode is mostly unstable for the coupled model except at very low turn rates. Whereas for the decoupled model, the spiral mode is always stable. This is due to the impact of the coupling terms L_u, $-q \sin\varphi - r \cos\varphi$ and is more prominent at higher turning rates where the value of is higher.

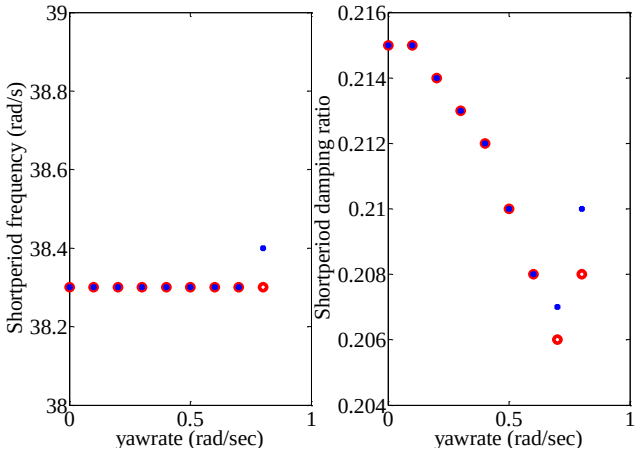

Figure 2 Short period mode for linear coupled (blue) and decoupled model (red) for steady turning flight

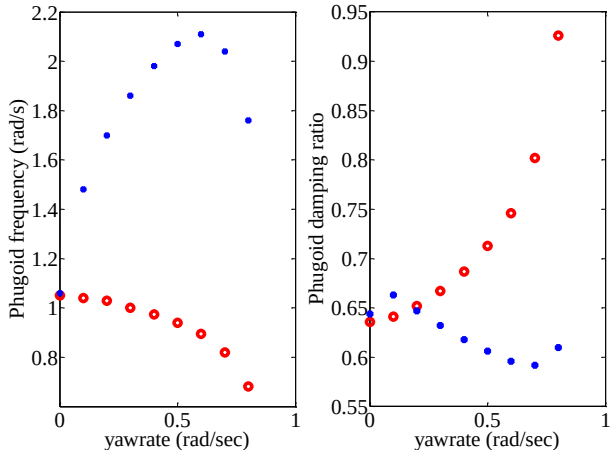

Figure 3 Phugoid mode for linear coupled (blue) and decoupled model (red) for steady turning flight

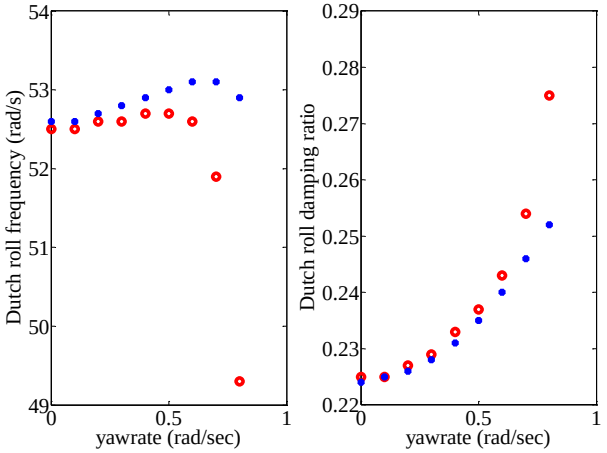

Figure 4 Dutch roll mode for linear coupled (blue) and decoupled model (red) for steady turning flight

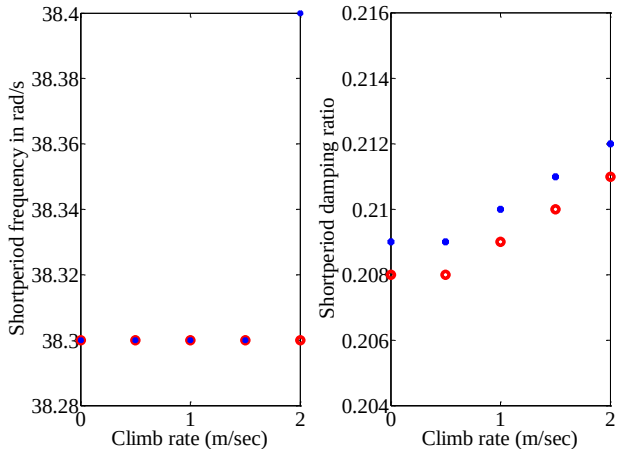

Figure 5 Short period mode for linear coupled (blue) and decoupled model (red) for steady turn and climbing flight

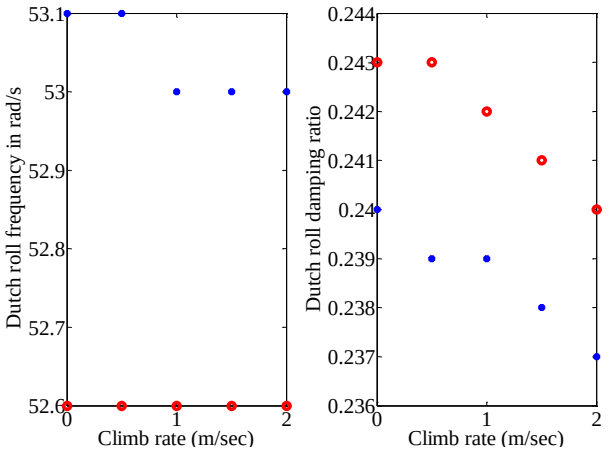

Figure 6 Dutch roll mode for linear coupled (blue) and decoupled model (red) for steady turn and climbing flight

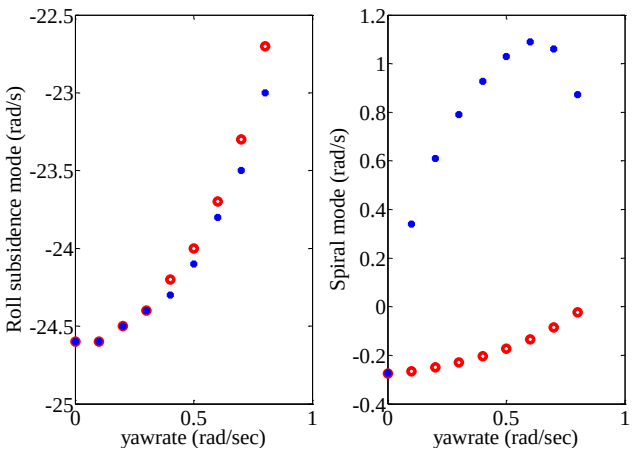

Figure 7 Roll subsidence and spiral modes for linear coupled (blue), and decoupled model (red) for steady turning flight

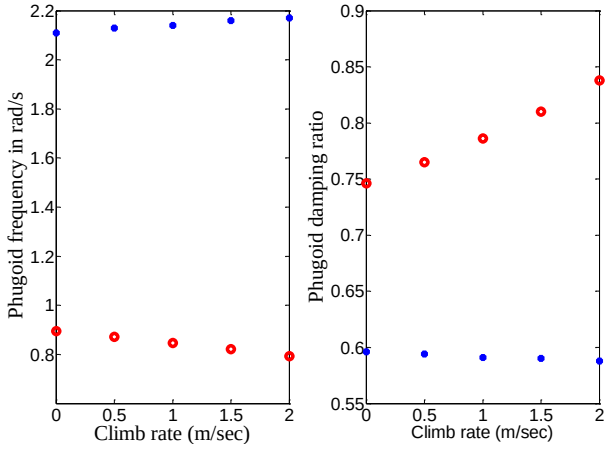

Figure 8 Phugoid mode for linear coupled (blue) and decoupled model (red) for steady turn and climbing flight

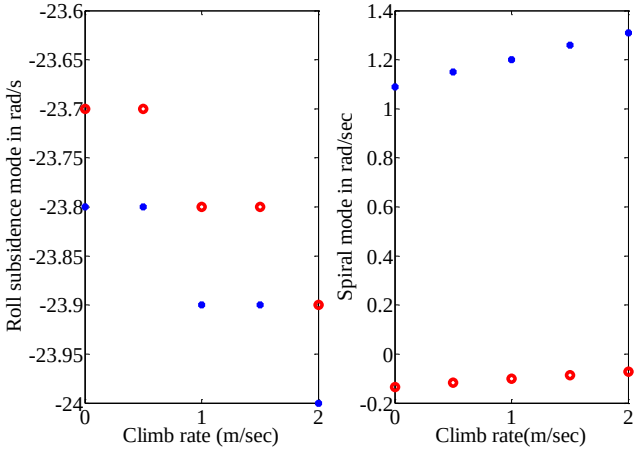

Figure 9 Roll subsidence and spiral modes for linear coupled (blue) and decoupled model (red) for steady turn and climbing flight

For the plant at V_a=12 m/s, turn rate of 0.6 rad/s and climb rate of 1 m/s, the eigen values of the coupled and decoupled model is given in **TABLE II** and the coupling matrices A_{longlat} and A_{latlong} are given in (30) and (31).

$$A_{longlat} = \begin{bmatrix} 0.2471 & 0 & 1.614 & 0 \\ -0.079 & -1.614 & 0 & -6.258 \\ 0.0473 & 0.4098 & -0.1116 & 0 \\ 0 & 0 & -0.6699 & -0.5713 \end{bmatrix} \quad (30)$$

$$A_{latlong} = \begin{bmatrix} -0.23 & -0.147 & 0 & -2.006 \\ 55.29 & 10.30 & -0.360 & 0 \\ -22.31 & -4.155 & 0.0373 & 0 \\ 0 & 0 & 0.2148 & 0.6301 \end{bmatrix} \quad (31)$$

TABLE II
Dynamic modes of the MAV for coupled and decoupled model

Dynamic modes	Coupled model	Decoupled model
Short period mode frequency, ω_{sp} (rad/s)	38.3	38.3
Short period mode damping ratio, ς_{sp}	0.210	0.209
Phugoid mode frequency, ω_{ph} (rad/s)	2.14	0.847
Phugoid mode damping ratio, ς_{ph}	0.591	0.786
Dutch roll mode frequency, ω_{dr} (rad/s)	53.0	52.6
Dutch roll mode damping ratio, ς_{dr}	0.239	0.242
Roll subsidence mode	-23.9	-23.8
Spiral mode	1.20(unstable)	-0.101(stable)

From **TABLE II**, it is evident that the coupled model shows unstable spiral mode but the decoupled model is unable to capture the unstable spiral mode. The reason for the unstable spiral mode can be explained as follows. The characteristic equation of the system given in (22) is

$$\begin{vmatrix} sI - A_{long} & -A_{longlat} \\ -A_{latlong} & sI - A_{lat} \end{vmatrix} = 0 \quad (32)$$

The eigen values are given by the roots of

$$\left|sI - A_{long}\right| \left|sI - A_{lat}\right| + \Delta\left(A_{longlat}, A_{latlong}\right) = 0 \quad (33)$$

where $\Delta\left(A_{longlat}, A_{latlong}\right)$ is a function of the coupling terms. The magnitude of the L_u term is higher when compared to other terms in the coupling matrix $A_{latlong}$ given in (31). Retaining only L_u and $-q\sin\varphi - r\cos\varphi$ among the coupling terms, (33) can be written as

$$\begin{aligned} &a_8 s^8 + a_7 s^7 + a_6 s^6 + a_5 s^5 + a_4 s^4 + a_3 s^3 \\ &+ a_2 s^2 + a_1 s^1 + a_0 + \Delta a_3 s^3 \\ &+ \Delta a_2 s^2 + \Delta a_1 s^1 + \Delta a_0 = 0 \end{aligned} \quad (34)$$

where coefficients a_0 to a_8 are the functions of decoupled matrices A_{long} and A_{lat}. The additional terms $\Delta a_3, \Delta a_2, \Delta a_1$ and Δa_0 appear due to the coupling terms L_u, $-q\cdot\sin\varphi - r\cdot\cos\varphi$ and are given by

$$\begin{aligned} \Delta a_3 &= L_u X_w(-q\sin\phi - r\cos\phi)(-g\sin\theta\cos\phi) \\ \Delta a_2 &= L_u(-q\sin\phi - r\cos\phi)\left((-g\sin\theta\cos\phi)\left(-X_q M_w - \left(M_q + Y_v + N_r\right)X_w\right) + g\cos\theta Z_q M_w\right) \\ \Delta a_1 &= L_u(-q\sin - r\cos\phi)\left[(Y_v + N_r)\left((-g\sin\theta\cos\phi)\left(X_w M_q - X_q M_w\right) + (-g\cos\theta)Z_q M_w\right) + X_w(-g\sin\theta\cos\phi)(Y_v N_r - Y_r N_v)\right] \\ \Delta a_0 &= (Y_v N_r - Y_r N_v)L_u(-q\sin\phi - r\cos\phi)\left[(g\sin\theta\cos\phi)\left(X_w M_q - X_q M_w\right) + (-g\cos\theta)Z_q M_w\right] \end{aligned} \quad (35)$$

In these coefficients, $(Y_v N_r - Y_r N_v)L_u(-g\cos\theta)Z_q M_w$ is much higher than the other terms in the expression of Δa_0, as result of that $\Delta a_3 > 0$, $\Delta a_2 > 0$, $\Delta a_1 > 0$ and $\Delta a_0 < 0$. The sum of the constant terms of the polynomial $\Delta a_0 + a_0$ is negative resulting in a positive root of the polynomial. The spiral mode is a function of N_v, N_r. The roll subsidence mode is a function of L_p. From (35), we can see that Δa_0 is a function of N_v, N_r, resulting in an unstable spiral mode. This motivates the control system design of the MAV needs to be based on the coupled model as against the conventional decoupled model.

III. Control System Design Specifications and The Selection of Nominal Model

A. *Control system design specifications*

The control system design specifications for the piloted aircraft are given by MIL-F-8785C standard [16]. It gives the requirement of minimum damping ratios of phugoid, short period and Dutch roll mode as 0.04, 0.35 and 0.19. Further, the spiral mode can be unstable with a minimum time to double as 4 seconds. These damping ratios are unacceptable for micro air vehicles, since they have higher natural frequencies when compared to the piloted aircraft. Moreover, unstable spiral mode will lead to mission failure if it is not stabilized by feedback control. Since the phugoid mode is the slowest, a minimum damping ratio of 0.40 is taken as the required value. For achieving higher phugoid damping [17], velocity feedback is required and the velocity measurements are not reliable in these classes of vehicles due to low precision differential pressure sensors. The minimum required closed loop damping ratios for Dutch roll mode and short period mode are taken as 0.45 as they have higher natural frequencies when compared to the phugoid mode. The closed loop spiral mode should be stable unlike in piloted aircraft. For MAVs, wind speeds are comparable to the flight velocity. So the closed loop system should reject the wind disturbances within the system bandwidth. Wind disturbances cause force as well as moment changes in MAV. It changes the angle of attack and sideslip angle and hence will affect the aerodynamic forces acting on the MAV. Here the disturbance rejection problem is modeled as a mixed sensitivity H_∞ optimization problem. The objective is to minimize the H_∞ norm of the output and control effort when the system is subject to wind disturbances.

B. Selection of the nominal model

The flight envelope of the MAV falls in the velocity range 9-19 m/s. The lack of accurate sensors to measure the flight velocity and angle of attack makes gain scheduling difficult in these classes of vehicles. So a single robust controller should handle the parameter variations within the entire flight envelope and plant model uncertainties. The selection of a linear nominal state space model for control system design can be done using μ analysis technique or ν- gap metric technique [9]. μ analysis identifies the worst case plant that is closer to instability. But here the spiral mode is already unstable so μ analysis cannot be used. Here ν- gap metric is used to identify the nominal model for the controller design. ν- gap metric is a norm that quantifies closeness of closed loop behavior of two plants when subjected to the same feedback control. It can be applied to unstable plants also. The ν- gap metric of two plants G_1 and G_2 can be defined as follows [18],

$$\delta_v(G_1, G_2) = \begin{cases} (I + G_2 G_2^*)^{-0.5}(G_1 - G_2)(I + G_1^* G_1)^{-0.5}, \\ \quad \text{if } det(I + G_2^* G_1) \neq 0, \forall \omega \\ \\ 1, \text{ otherwise} \end{cases} \tag{36}$$

In (36), det() denotes the determinant and G_1^* represents the complex conjugate of G_1 and ω represents the frequency. The value of ν- gap metric of two plants lies between 0 and 1. If the value of ν- gap metric is closer to 0, then a single controller can generate almost same closed loop behavior for both the plants. If the value of ν- gap metric is closer to 1, then the closed loop behavior of the two plants will differ drastically in response to the same controller. The ν- gap metric can be computed using the MATLAB command *gapmetric*.

TABLE III
The ν- gap metric value, Va = 9-19 m/s

Velocity (m/s)	MeMean ν- gap metric
9	0.9605
10	0.9591
11	0.9864
12	0.7379
13	0.5646
14	0.5123
15	0.4913
16	0.4847
17	0.4928
18	0.5154
19	0.5528

TABLE IV
The ν- gap metric value for climbing flight

$\dot{h}$ (m/s)	Mean ν- gap metric
0.0	0.0249
0.5	0.0175
1.0	0.0150
1.5	0.0175
2.0	0.0251

The ν- gap metric is obtained for linearized plants at different operating conditions, choosing one plant as nominal plant. The mean ν- gap metric value for linearized state space models obtained for steady turn condition is shown in **TABLE III**. The velocity is varied from 9 m/s to 19 m/s and the turn rate is fixed as 0.6 rad/s. The turn rate of 0.6 rad/s corresponds to the worst case spiral mode of 1.09 as in **Figure 7**. From the **TABLE III**, the smallest mean ν- gap metric value is for the plant at V_a=16 m/s. The plant at V_a=16 m/s with a turn rate of 0.6 rad/s is further analyzed for different climb rates varying from 0 m/s to 2 m/s as shown in **TABLE IV**. Finally the plant at V_a=16 m/s, turn rate of 0.6 rad/s and a climb rate of 1 m/s is taken as the nominal model and the state space model is given by

$$\dot{X} = AX + BU$$
$$Y = CX$$

where $X = \begin{bmatrix} X_{long} & X_{lat} \end{bmatrix}^T$, $B = \begin{bmatrix} B_{long} & B_{lat} \end{bmatrix}^T$ are as given in (22).

$U = [\, \delta_e \; \delta_r \; \delta_{Th} \,]^T$, and $Y = [\widetilde{a_x} \quad \widetilde{a_z} \quad \tilde{q} \quad \widetilde{a_y} \quad \tilde{p} \quad \tilde{r}]^T$

$$A = \begin{bmatrix} A_{long} & A_{longlat} \\ A_{latlong} & A_{lat} \end{bmatrix}$$

where

$$A_{long} = \begin{bmatrix} -1.6008 & 1.0090 & -1.8248 & -9.6677 \\ -0.3625 & -7.3539 & 15.6104 & -1.1383 \\ 19.11 & -158.34 & -15.238 & 0 \\ 0 & 0 & 0.6838 & 0 \end{bmatrix}$$

$$A_{longlat} = \begin{bmatrix} 0.3405 & 0 & -0.6 & 0 \\ 0.0384 & 0.6 & 0 & -7.0544 \\ 0.0155 & 0.3812 & -0.0402 & 0 \\ 0 & 0 & -0.7297 & 0.5913 \end{bmatrix}$$

$$A_{latlong} = \begin{bmatrix} -0.3378 & -0.094 & 0 & -1.215 \\ 49.73 & 5.871 & -0.337 & 0 \\ -6.363 & -0.7512 & 0.0061 & 0 \\ 0 & 0 & 0.1256 & 0.6088 \end{bmatrix}$$

$$A_{lat} = \begin{bmatrix} -3.5439 & 1.7538 & -15.493 & 6.6106 \\ -412.85 & -29.48 & 27.502 & 0 \\ 245.34 & -4.79 & -30.038 & 0 \\ 0 & 1 & 0.1177 & 0 \end{bmatrix}$$

$$B = \begin{bmatrix} 5.16 & 0 & 0.197 \\ -70 & 0 & 0 \\ -6850 & 0 & 0 \\ 0 & 0 & 0 \\ 0 & 38.7 & 0 \\ 0 & 12838 & 0 \\ 0 & -2982.4 & 0 \\ 0 & 0 & 0 \end{bmatrix}$$

$$C = \begin{bmatrix} 0 & 0.4 & 1.8 & 9.6 & -0.4 & 0 & -0.6 & 0 \\ -0.4 & 0 & -15.8 & 1.1 & -0.1 & 0.6 & 0 & 7.1 \\ 0 & 0 & 1 & 0 & 0 & 0 & 0 & 0 \\ 0.4 & 0.1 & 0 & 1.2 & 0 & -1.8 & 15.8 & -6.6 \\ 0 & 0 & 0 & 0 & 0 & 1 & 0 & 0 \\ 0 & 0 & 0 & 0 & 0 & 0 & 1 & 0 \end{bmatrix}$$

The short period, phugoid and other modes of the nominal coupled plant at V_a = 16 m/s , turn rate of 0.6 rad/s and a climb rate of 1 m/s are given in **TABLE V**.

TABLE V
Dynamic modes of the MAV for the nominal model

Dynamic modes	Open loop
Short period mode frequency, ω_{sp} (rad/s)	51.2
Short period mode damping ratio, ς_{sp}	0.221
Phugoid mode frequency, ω_{ph} (rad/s)	2.15
Phugoid mode damping ratio, ς_{ph}	0.663
Dutch roll mode frequency, ω_{dr} (rad/s)	69.0
Dutch roll mode damping ratio, ς_{dr}	0.215
Roll subsidence mode	-33.2
Spiral mode	1.13 (unstable)

We can see that the short period and Dutch roll damping ratio is poor and the spiral mode is unstable.

IV. H_∞ Control Formulation

Mixed sensitivity H_∞ control is used when sensitivity function (S) is shaped along with complementary sensitivity function (T) or transfer function like KS [19]. Here we have a regulation problem in which, the objective is to reject the wind disturbance while using a minimum actuator effort. S is the transfer function between the output and disturbance input and KS is the transfer function between the control input and disturbance input. The control design objective is to find a static output feedback gain $u_c = Ky$ such that the norm

$$\|T_{zw}\|_\infty = \left\| \begin{matrix} W_1 S \\ W_2 KS \end{matrix} \right\|_\infty \quad (37)$$

is minimized. The sensitivity function (S) should be minimized at lower frequencies to reject disturbances affecting the plant. The weight $W_1(s)$ is taken as low pass filter to minimize S at lower frequencies and $W_2(s)$ is taken as high pass filter to limit the control effort at higher frequencies. The block diagram of the mixed sensitivity H_∞ control problem is given in **Figure 10**. Here $w = w_d$ is the disturbance input, u_c is the control input, $z=[z_1, z_2]$ is the performance output , y is the measured variable, G_p is the plant transfer function and G_d is the disturbance transfer function. After augmenting the nominal plant with the weighting transfer functions, the state space equation of the generalized plant is given by

$$\begin{aligned} \dot{x} &= Ax + Bu_c + B_w w_d \\ z_1 &= C_1 x + D_{11} u_c + D_{12} w_d \\ z_2 &= C_2 x + D_{21} u_c + D_{22} w_d \\ y &= Cx \end{aligned} \quad (38)$$

where

$$x \in R^{n_g},\ y \in R^{p_g}, u_c \in R^{m_g}, \\ w_d \in R^{d_g}, z_1 \in R^{z_{1g}}, z_2 \in R^{z_{2g}}$$

and

$$W_1 = \begin{bmatrix} w_{11} & 0 & 0 & 0 & 0 & 0 \\ 0 & w_{12} & 0 & 0 & 0 & 0 \\ 0 & 0 & w_{13} & 0 & 0 & 0 \\ 0 & 0 & 0 & w_{14} & 0 & 0 \\ 0 & 0 & 0 & 0 & w_{15} & 0 \\ 0 & 0 & 0 & 0 & 0 & w_{16} \end{bmatrix}$$

$$W_2 = \begin{bmatrix} w_{21} & 0 & 0 \\ 0 & w_{22} & 0 \\ 0 & 0 & w_{23} \end{bmatrix}$$

Here n_g is the order of the generalized plant, p_g is the number of measurements, m_g is the number of control inputs, d_g is the number of disturbance inputs, z_{1g} is the number of performance output z_1 and z_{2g} is the number of performance output z_2. From (38),

$$y(s) = C[sI - A]^{-1}Bu_c + C[sI - A]^{-1}B_w w_d \quad (39)$$

From figure 10,

$$y(s) = G_p u_c + G_d w_d \quad (40)$$

From (39) and (40),

$$\begin{aligned} G_p &= C[sI - A]^{-1}B \\ G_d &= C[sI - A]^{-1}B_w \end{aligned} \quad (41)$$

$$\|T_{zw}\|_\infty = \left\| \begin{matrix} W_1 G_p K[I - G_p K]^{-1} G_d \\ W_2 K[I - G_p K]^{-1} G_d \end{matrix} \right\|_\infty \quad (42)$$

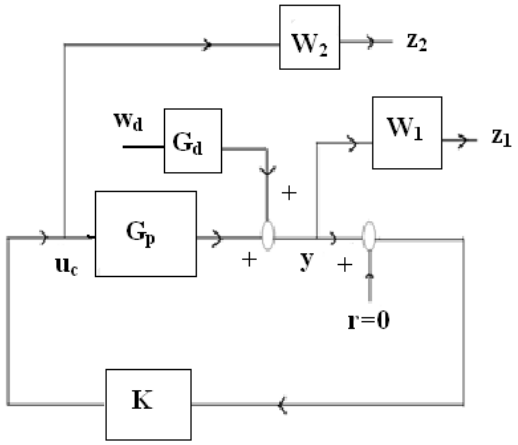

Figure 10 Block diagram of mixed sensitivity H∞ control problem

V. Discrete Static Output Feedback Control

For the ease of practical implementation and to handle sampling inaccuracies and quantization effects, the controller is designed directly in the digital domain. The discrete time representation for the generalized plant given in (38) is written as

$$\begin{aligned} x(k+1) &= Ax(k) + Bu_c(k) + B_w w_d(k) \\ z_1(k) &= C_1 x(k) + D_{11} u_c(k) + D_{12} w_d(k) \\ z_2(k) &= C_2 x(k) + D_{21} u_c(k) + D_{22} w_d(k) \\ y(k) &= Cx(k) \end{aligned} \tag{43}$$

To stabilize the plant in (43) with a controller $u(k) = Ky(k)$, the Lyapunov condition [20] is

$$\exists P > 0, \ni (A + BKC)^T P (A + BKC) - P < 0 \tag{44}$$

For placing the poles inside a circle of radius λ where $\lambda < 1$ and $\lambda^2 = \mu$, the Lyapunov equation can be modified as [20],

$$(A + BKC)^T P (A + BKC) - \mu P < 0 \tag{45}$$

Lemma [21]: The Lyapunov equation $A^T P A - P < 0$ can be written as

$$\begin{bmatrix} P & A^T X^T \\ XA & -P + X + X^T \end{bmatrix} > 0 \tag{46}$$

where X is any symmetric matrix. Using the above result, (45) can be written as

$$\begin{bmatrix} \mu P & (A + BKC)^T X^T \\ X(A + BKC) & -P + X + X^T \end{bmatrix} > 0 \tag{47}$$

$$\begin{bmatrix} -\mu P & -(A + BKC)^T X^T \\ -X(A + BKC) & P - X - X^T \end{bmatrix} < 0 \tag{48}$$

The Bilinear Matrix Inequality (BMI) in (45) is transformed into a Linear Matrix Inequality (LMI) for a fixed value of X. The variable X is obtained using genetic algorithm (GA). GA is an evolutionary algorithm that uses probabilistic search techniques to minimize a performance index. The algorithm for obtaining the static output feedback gain is given below

1) Choose X as the decision variable for the genetic algorithm. The performance index (PI) can be formulated based on the closed loop damping requirements and $\|T_{zw}\|_\infty$

   IF A+BKC is not stable, then PI = 10000 (a very high value),
   ELSEIF closed loop poles damping ratio < required damping ratio,
   then PI = 5000,
   Else PI = $\|T_{zw}\|_\infty$,
   END

2) For an initial X given by the genetic algorithm, solve the LMI in (48) to obtain P and K

3) Obtain the closed loop matrix A+BKC and evaluate the PI as given in step 1.

4) Run the GA until a satisfactory solution is obtained. Here, more penalty is given in the performance index for violating the closed loop stability requirements, since the open loop plant is unstable.

VI. Integrated Guidance And Control

In conventional guidance and control, three separate navigation, guidance, and control loops are designed in a hierarchical way. In integrated guidance and control, there are no separate loops and hence spectral separation between the inner loop and outer loop is not needed. The control input is generated such that vehicle moves from one waypoint to another with robustly maintaining the stability of the vehicle. Here the path connecting the waypoints is broken into discrete points along the path and each point one by one is tracked by the IGC algorithm.

Here the sensor output of the MAV and reference path is used by the IGC algorithm to generate the control input. The system input takes a form of $U = F_i(X) + G_i(d)$, where d is the miss distance vector and is computed in a single step. The output of the MAV are the accelerometer output a_x,a_y,a_z, gyro output p,q,r, air speed V_a, GPS output x,y,z and heading Ψ. The miss distance vector can be obtained using the current MAV position, velocity vector and the next point in the path to be followed. The control inputs are the elevator, rudder and throttle. The variables d_1, d_3 are the projection of miss distance vector in MAV pitch plane and yaw plane respectively. The variables d_2, d_4 are the derivatives of d_1, d_3 respectively. The objective is to maintain a near constant air speed and to drive the miss distance to zero. The miss distance variables are linearized and added to the state space equation given in (22) to form a twelve state model. The linear state space model of IGC is given by

$$\begin{aligned} \dot{X}_I &= A_I X_I + B_I U_I \\ Y_I &= C_I X_I \end{aligned} \tag{49}$$

$$X_I = [\tilde{u} \quad \tilde{w} \quad \tilde{q} \quad \tilde{\theta} \quad \widetilde{d_1} \quad \widetilde{d_2} \quad \tilde{v} \quad \tilde{p} \quad \tilde{r} \quad \tilde{\phi} \quad \widetilde{d_3} \quad \widetilde{d_4}]^T$$

where, $U_I = [\ \delta_e \ \delta_r \ \delta_{Th}\ ]^T$ and

$$Y_I = \left[\widetilde{a_x} \quad \widetilde{a_z} \quad \tilde{q} \quad \widetilde{d_1} \quad \widetilde{V_a} \quad \widetilde{a_y} \quad \tilde{p} \quad \tilde{r} \quad \widetilde{d_3}\right]^T \tag{50}$$

For the nominal plant model at V_a=16 m/s , turn rate of 0.6 rad/s and a climb rate of 1 m/s, the open loop poles are given in **TABLE VI**.

TABLE VI
Dynamic modes of twelve state IGC model

Dynamic modes	Open loop
Short period mode frequency, ω_{sp} (rad/s)	51.2
Short period mode damping ratio, ς_{sp}	0.221
Phugoid mode frequency, ω_{ph} (rad/s)	2.15
Phugoid mode damping ratio, ς_{ph}	0.663
Dutch roll mode frequency, ω_{dr} (rad/s)	69.0
Dutch roll mode damping ratio, ς_{dr}	0.215
Roll subsidence mode	-33.2
Spiral mode	1.13 (unstable)
Poles corresponding to $\widetilde{d_1}, \widetilde{d_2}, \widetilde{d_3}, \widetilde{d_4}$	0,0,0,0

The miss distance variables $\widetilde{d_1}, \widetilde{d_2}, \widetilde{d_3}, \widetilde{d_4}$ adds integrator to the model. The miss distance variables can be obtained as follows.

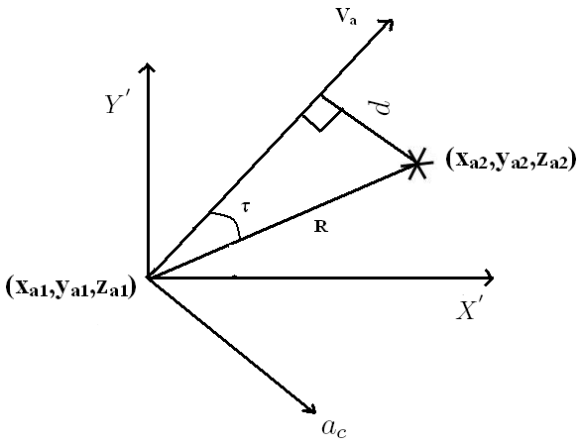

Figure 11 Diagram showing the miss distance

Let the unit vector along current velocity vector of the MAV be (cosΨcosγ, sinΨcosγ, sinγ), where Ψ is the heading angle and γ is the flight path angle of the MAV. In **Figure 11**, V_a is the magnitude of the current velocity vector of the MAV, (x_{a1},y_{a1},z_{a1}) is the current position of the MAV, (x_{a2},y_{a2},z_{a2}) is the next point where MAV has to reach, R is the distance vector, a_c is the applied acceleration , X'Y' is the axis of the plane defined by the velocity vector and R. The angle between the velocity vector and R is τ. The miss distance vector d is the vector perpendicular to the velocity vector drawn from the vector R at (x_{a2},y_{a2},z_{a2}). The applied acceleration a_c is proportional to the miss distance d and is applied perpendicular to the velocity vector. The miss distance d can be obtained as

$$d = R \sin\tau \tag{51}$$

where

$$R = \sqrt{(x_{a1}-x_{a2})^2 + (y_{a1}-y_{a2})^2 + (z_{a1}-z_{a2})^2}$$

In **Figure 12**, XZ is the pitch plane of the MAV, X_B denotes the body X axis, α is the angle of attack, γ is the flight path angle and $V_a\dot{\gamma}$ is the acceleration perpendicular to the velocity vector in the pitch plane. Let the unit vector along the applied acceleration vector ac be (a_{m1}, b_{m1}, c_{m1}). The acceleration component in the MAV pitch plane and yaw plane are approximated as the second derivative of the miss distance. The angle made by the acceleration vector with the X axis in the pitch plane is given by

$$\gamma_{a1} = \tan^{-1}\left(\frac{c_{m1}}{\sqrt{{a_{m1}}^2+{b_{m1}}^2}}\right) \tag{52}$$

$$\ddot{d_1} = -a_c \sin\gamma_{a1} \tag{53}$$

$$a_c \sin\gamma_{a1} = V_a\dot{\gamma}\cos\gamma \tag{54}$$

Let $\dot{d_1} = d_2$, then from (52) to (54),

$$\dot{d_2} = -V_a\dot{\gamma}\cos\gamma \tag{55}$$

In **Figure 13**, XY is the yaw plane of the MAV, X_B denotes the body X axis, β is the sideslip angle, Ψ is the yaw angle and $V_a(\dot{\Psi}+\dot{\beta})$ is the acceleration perpendicular to the velocity vector in the yaw plane. The angle made by the acceleration vector a_c with the X axis in the yaw plane is given by

$$\Psi_{a1} = \tan^{-1}\left(\frac{b_{m1}}{a_{m1}}\right) \tag{56}$$

$$\ddot{d_2} = -a_c\cos\gamma_{a1} \tag{57}$$

$$a_c\cos\gamma_{a1}\cos\Psi_{a1} = V_a(\dot{\Psi}+\dot{\beta})\sin(\Psi+\beta) - V_a\dot{\gamma}\sin\gamma \tag{58}$$

$$a_c\cos\gamma_{a1}\sin\Psi_{a1} = -V_a(\dot{\Psi}+\dot{\beta})\cos(\Psi+\beta) \tag{59}$$

Let
$\dot{d_3} = d_4$ and $\Psi+\beta = \lambda$, then from (56) to (59),

$$\dot{d_4} = -V_a\sqrt{\lambda^2 - 2\dot{\gamma}\dot{\lambda}\sin\gamma\sin\lambda + (\dot{\gamma}\sin\gamma)^2} \tag{60}$$

The applied acceleration a_c is parallel to the miss distance *d*,

$$d_1 = d\sin\gamma_{a1} \text{ and } d_2 = d\cos\gamma_{a1} \tag{61}$$

The objective is to achieve zero miss distance, so as to track the desired reference path. Zero miss distance implies that either the MAV has reached the desired waypoint or the velocity vector of the MAV is pointing towards the desired waypoint. The basic block diagram of IGC is given in Figure 14. Further details of integrated guidance and control can be found in [22].

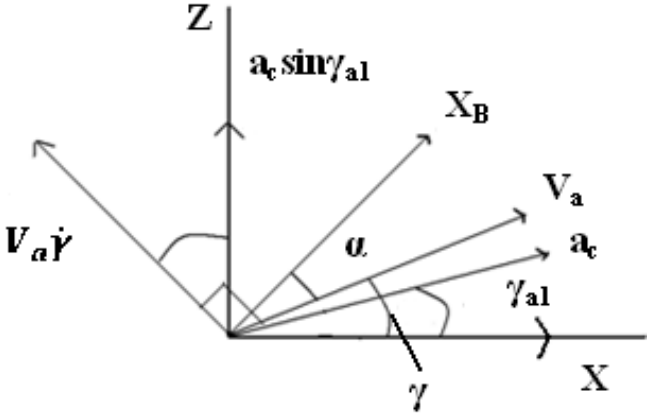

Figure 12 Acceleration component in the MAV pitch plane

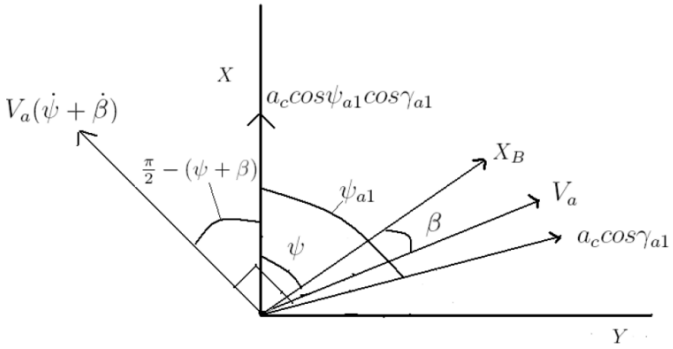

Figure 13 Acceleration component in the MAV yaw plane

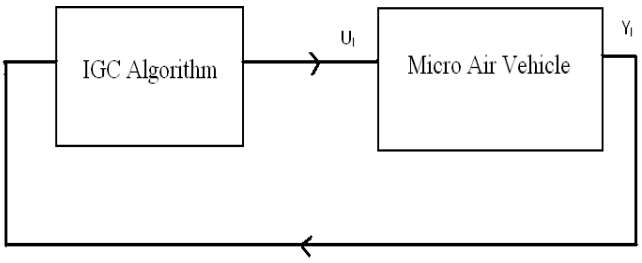

Figure 14 Basic block diagram of IGC

VII. SIMULATION RESULTS

The weighting function $W_1(s)$ is used to minimize the sensitivity over the frequency band where the disturbances are prominent [19]. So $W_1(s)$ is taken as low pass filter to reject low frequency disturbances. The weighing function $W_2(s)$ minimizes the control effort at high frequencies. The weighing function $W_2(s)$ is taken as a high pass filter with cutoff frequency as a function of actuator amplitude and rate saturation [23]. The range for control actuation are [-35°,+15°] for the elevator deflection, [-25°,+25°] for the rudder deflection and 0-12000 rpm for the BLDC motor-propeller system. The actuator is modeled as a second order system with a natural frequency of 48.6 rad/s and a damping ratio of 0.74. The poles of the weights are taken based on the open loop dynamic modes of the plant. For the weights

$$W_1(s) = \text{diag}\left(\frac{1}{s+50}, \frac{1}{s+50}, \frac{1}{s+50}, \frac{1}{s+70}, \frac{1}{s+35}, \frac{1}{s+70}\right)$$

and

$$W_2(s) = \text{diag}\left(\frac{0.1s+1}{s+50}, \frac{0.1s+1}{s+70}, \frac{0.1s+1}{s+50}\right)$$

The controller gain matrix is given in (62).

$$K = \begin{bmatrix} -0.053 & -0.0169 & -0.2642 & -0.0036 & 0.0046 & 0.0524 \\ 0.0010 & 0.0171 & 0.2713 & 0.0032 & -0.0046 & -0.0542 \\ 0.2053 & 16.971 & 229.9 & -11.06 & 11.70 & -13.51 \end{bmatrix} \quad (62)$$

The closed loop natural frequencies and damping ratios are given in **TABLE VII**. The sampling frequency used is 50 Hz. We can see that the closed loop damping ratio has been improved for short period and Dutch roll mode and more importantly, the spiral mode has been stabilized. Wind disturbances cause force as well as moments in MAV. It changes the angle of attack and sideslip angle and hence will affect the aerodynamic forces acting on the MAV. In state space model, u is replaced by $u+u_w$, v is replaced by $v+v_w$, and w is replaced by $w+w_w$. For the vector of angular velocities, p is influenced by the wind most and hence p is replaced by $p+p_w$ [24]. A sinusoidal disturbance of frequency 80 rad/s and 65 rad/s corresponding to the closed loop Dutch roll and short period frequency has been applied to the open loop linear plant and the closed loop linear plant.

The responses are given from **Figure 15** to Figure 20. The red curve represents the open loop system and the blue curve represents the closed loop system. We can see that the closed loop plant is attenuating the disturbance whereas the open loop plant is diverted to instability due to unstable spiral mode. Similar methodology has been adopted for the control design in IGC framework. The weighting function $W_1(s)$ is taken as low pass transfer function to minimize the sensitivity.

TABLE VII
Closed loop dynamic modes of the MAV

Dynamic modes	Closed loop
Short period mode frequency, ω_{sp} (rad/s)	65.3
Short period mode damping ratio, ς_{sp}	0.47
Phugoid mode frequency, ω_{ph} (rad/s)	0.73
Phugoid mode damping ratio, ς_{ph}	0.85
Dutch roll mode frequency, ω_{dr} (rad/s)	80.4
Dutch roll mode damping ratio, ς_{dr}	0.45
Roll subsidence mode	-23.7
Spiral mode	-14.1

The miss distance variables $\widetilde{d_1}, \widetilde{d_2}, \widetilde{d_3}, \widetilde{d_4}$ add poles at the origin. This makes the overall response of the system sluggish. So the weighting functions of control effort $W_2(s)$ are modified to enhance the transient response. The weights are given by

$$W_1(s) = \text{diag}\left(\frac{1}{s+50}, \frac{1}{s+50}, \frac{1}{s+50}, \frac{1}{s+50}, \frac{1}{s+100}, \frac{1}{s+70}, \frac{1}{s+35}, \frac{1}{s+70}, \frac{1}{s+100}\right)$$

and

$$W_2(s) = \text{diag}\left(\frac{0.1(s+1)}{s+5}, \frac{0.1(s+1)}{s+6}, \frac{0.02(s+5)}{s+6}\right)$$

The closed loop poles obtained are given in **TABLE VIII** for the controller gain matrix given in (63). The miss distance in the pitch plane and yaw plane for the closed loop system for an initial value of 5 m and 4 m are given in **Figure 21** and **Figure 22** respectively.

$$K_I = \begin{bmatrix} 0.013 & -0.0104 & -2.02 \\ -0.109 & 0.067 & 10.12 \\ -1.76 & 1.08 & 164.4 \\ 0.0034 & -0.011 & -2.34 \\ 0.0002 & -0.0002 & 0.34 \\ -0.12 & 0.073 & -0.11 \\ -0.22 & 0.14 & 20.4 \\ 1.85 & -1.17 & -175.2 \\ -0.002 & -0.002 & -0.33 \end{bmatrix} \quad (63)$$

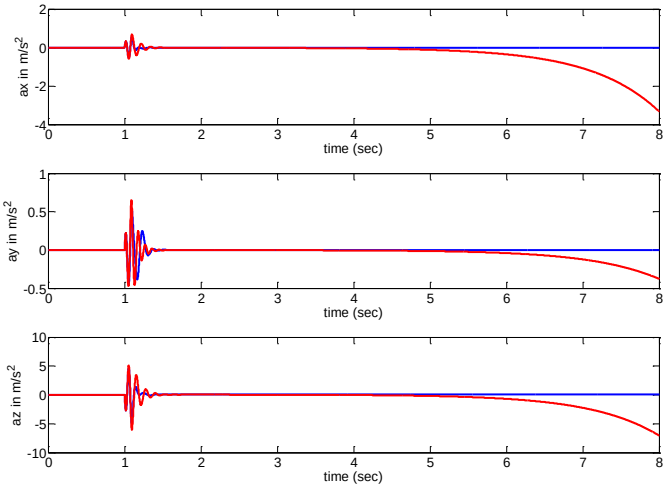

Figure 15 Acceleration output for a sinusoidal disturbance of freq. 80 rad/sec (red—open loop, blue—closed loop)

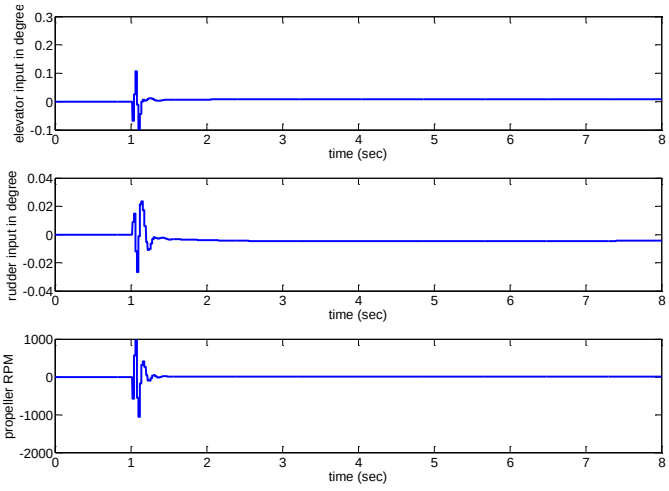

Figure 16 Control effort for a sinusoidal disturbance of freq. 80 rad/sec

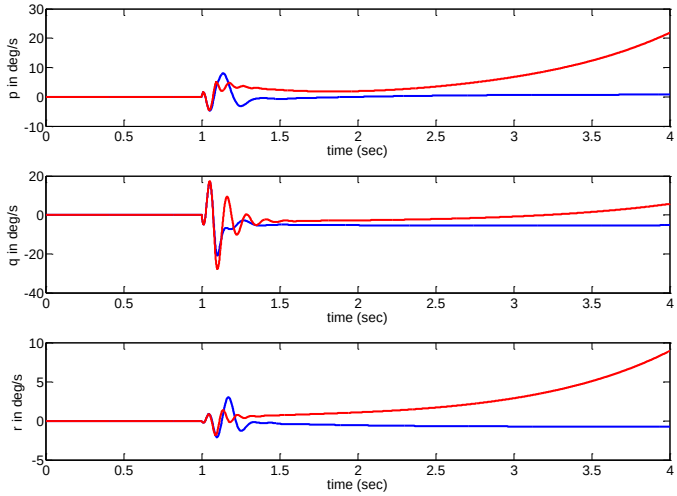

Figure 17 Angular rates output for a sinusoidal disturbance of freq. 65 rad/sec (red-open loop, blue-closed loop)

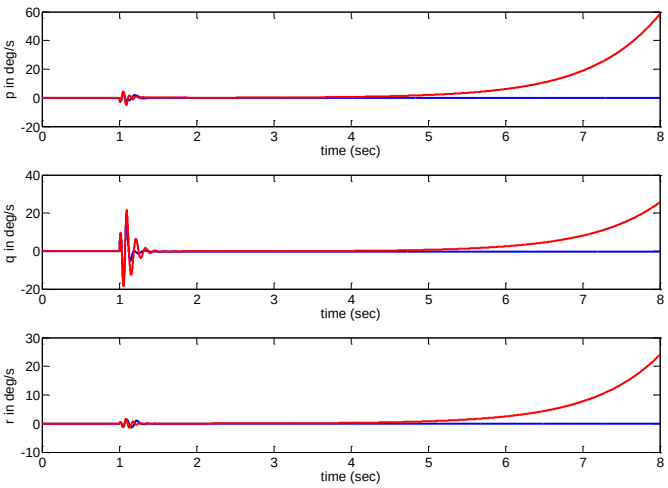

Figure 18 Angular rates output for a sinusoidal disturbance of freq. 80 rad/sec (red—open loop, blue—closed loop)

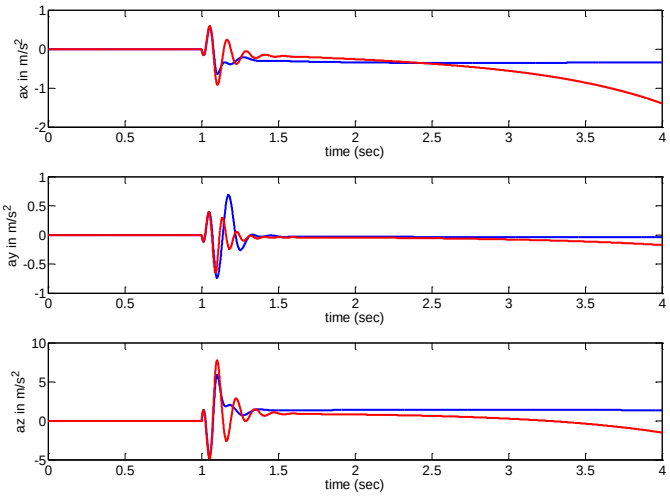

Figure 19 Acceleration output for a sinusoidal disturbance of freq. 65 rad/sec (red—open loop, blue—closed loop)

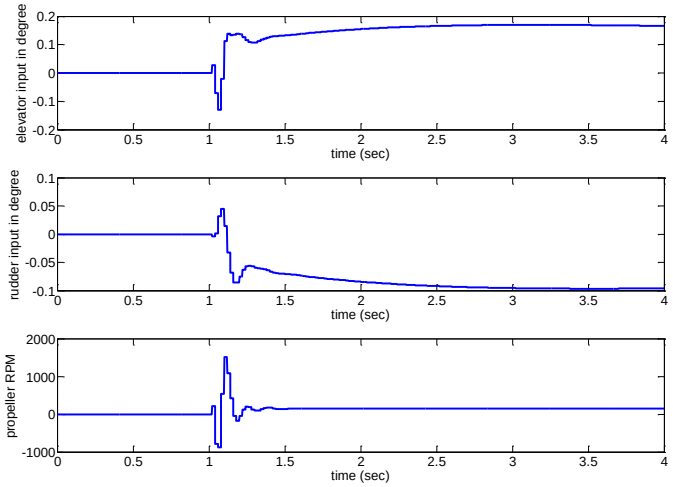

Figure 20 Control effort for a sinusoidal disturbance of freq. 65 rad/sec

TABLE VIII
Closed loop dynamic modes of IGC model

Dynamic modes	Closed loop
Short period mode frequency, ω_{sp} (rad/s)	67.2
Short period mode damping ratio, ς_{sp}	0.44
Phugoid mode frequency, ω_{ph} (rad/s)	1.72
Phugoid mode damping ratio, ς_{ph}	0.73
Dutch roll mode frequency, ω_{dr} (rad/s)	91.8
Dutch roll mode damping ratio, ς_{dr}	0.42
Roll subsidence mode	-27.8
Spiral mode	-4.51
Poles corresponding to $\widetilde{d_1}, \widetilde{d_2}, \widetilde{d_3}, \widetilde{d_4}$	-0.35, -0.09, -0.11, -1.9

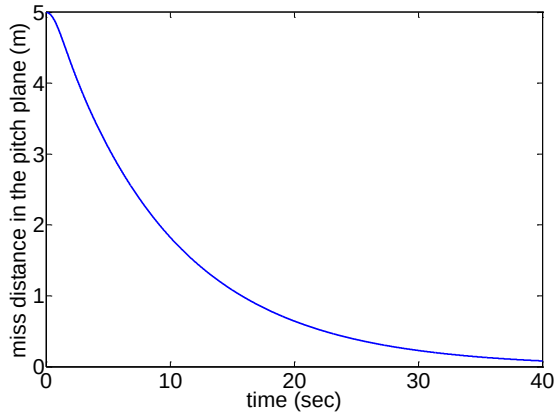

Figure 21 Miss distance in the pitch plane for IGC closed loop system

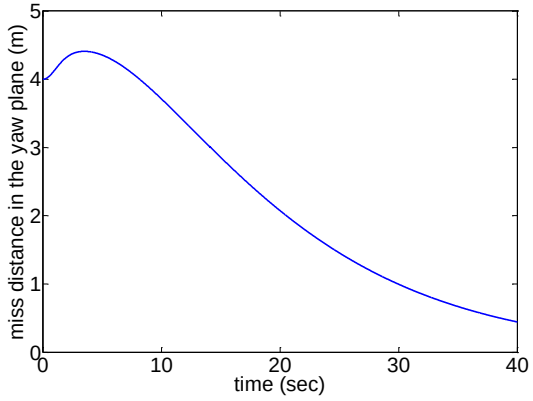

Figure 22 Miss distance in the yaw plane for IGC closed loop system

VIII. CONCLUSIONS

In this paper, the strong coupling between the longitudinal and lateral dynamics of a 150 mm MAV is addressed. It is shown that the combined longitudinal and lateral model can capture the unstable spiral dynamics. The ν- gap analysis is used to obtain the nominal plant for control system design from a set of unstable plants. A discrete static output feedback controller is designed using LMI and genetic algorithm. The resulting controller stabilizes the spiral mode and provides good short period and Dutch roll damping. The simulation results show that the mixed H_∞ control formulation provides good disturbance rejection. The controller design is also done for a novel twelve-state integrated guidance and control framework.

ACKNOWLEDGMENT

This study is funded by the NP-MICAV program of ARDB/DRDO. The authors would also like to thank Mr. Jinraj V Pushpangathan, Mr. Sidhant Dhall , Mr. Titas Bera and Mr. Eobin Alex George for their support.

REFERENCES

[1] D. Siqueria , P. Paglione , and F.J.O Moreira,"Robust Fixed Structure Output Feedback Flight Control Law Synthesis and Analysis Using Singular Structured Value," *Aerospace Science and Technology* , Vol.30, pp.102–107, 2013. CrossRef

[2] J. Gadewadikhar, F. L. Lewis, K. Subharo and B.M Chen, "Design of H_∞ Command and Control Loops for Unmanned Aerial Vehicles using Static Output-Feedback,"*46Th IEEE Conference on Decision and Control*, Vol. 1, pp. 5395–5400, USA, 2007.

[3] J.Gadewadikar, F.L.Lewis and M.AbuKhalaf, "Necessary and Sufficient Conditions for H_∞ Static Output-Feedback Control," *Journal of Guidance Dynamics and Control*, Vol. 29, pp. 915-921, 2006. CrossRef

[4] J. Gadewadikar, F. L. Lewis, "Aircraft Flight Controller tracking design using H_∞ Static Output-Feedback," *Transactions of the Institute of Measurement and Control*, Vol. 28, No. 5, pp. 429-440, 2006. CrossRef

[5] J. Gadewadikar, F. L. Lewis, V. Kucera, L. Xie, and M. AbuKhalaf ,"Parameterization of All Stabilizing H∞ Static State-Feedback Gains:Application to Output-Feedback Design," *Automatica*, Volume 43,Issue 9, pp. 1597-1604, September 2007. CrossRef

[6] D. Nuemann, and H.X. de Araujo , "Hybrid Differential Evolution method for the Mixed H_2/H_∞ Robust Control Problem under Pole Assignment,", *44Th IEEE Conference on Decision and Control and the European Union Conference* ,Vol. 19, pp. 1319 -1324, Spain, 2005.

[7] R.Toscano, and P.Lyonnet, "Robust static output feedback controller synthesis using Kharitonov's theorem and evolutionary algorithms," *Journal of information Sciences* , Vol.180, pp.2023-2028, 2010. CrossRef

[8] Y.Kong, D. Zhau, B.Yang, T.Shen , H. Li and K.Han , "Static Output Feedback Control for Active Suspension Using PSO-DE/LMI Approach," *Internalional Confernce on Mechatronics and Automation* , IEEE, pp. 366-370, China, 2012.

[9] S.I. Alswailem, "Air Vehicle Modeling Uncertainity and the v-Gap Metric ," *control 2004* ,University of Bath, UK, ID-213, September 2004.

[10] N.Kannan, M. Seetharama Bhat , "Longitudinal H_∞ stability augmentation system for a thrust vectored unmanned aircraft", *Journal of Guidance Control and Dynamics*, Vol.28, No.6, pp.1240-1250, 2005. CrossRef

[11] M. Meenakshi, M. Seetharama Bhat," Robust fixed order H_2 controller for micro air vehicle- design and validation", *Optimal Control Applications and Methods*, Vol.27, No.1, pp.183-210, 2006. CrossRef

[12] Neha Satak, M. Seetharama Bhat ," Modified ILMI algorithm for practical PID/PD implementation on a micro air vehicle", *American control Conference*, pp.4660-4665, 2009.

[13] S. Karthik, " Robust L_1 adaptive control of micro air vehicle", *ME Thesis, Department of Aerospace Engineering, Indian Institute of Science*, Bangalore-2013.
[14] R.W. Beard, T.W. Mclain, "*Navigation, Guidance and Control of Small Unmanned Aircraft*", Princeton University Press, New Jersey, 2009.
[15] W.F. Phillips, "*Mechanics of flight*", Wiley India, pp. 924-934, 2010.
[16] B.L. Stevens, F.L. Lewis, "*Aircraft control and simulation*", John Wiley and Sons, pp.222-236, 1992.
[17] J.H. Blakelock, " *Automatic control of aircraft and missiles*", John Wiley and Sons, pp.87, 1991.
[18] K. Zhou, J.C. Doyle, "Essentials of robust control", Prentice hall, pp.349-367, 1998.
[19] S. Skogestad, I.Postlethwaite, " *Multivariable feedback control , Analysis and design*" John Wiley and Sons, pp. 394, 2001.
[20] G.F. Franklin, J.D. Powell , M. Workman, "*Digital control of dynamic systems*", Pearson education, Asia, 2002.
[21] M.C. Oliveira, J.Bernussou, J.C. Geromel, " A new discrete-time robust stability condition", *Systems and Control Letters*, 37, pp. 261-265, 1999. CrossRef
[22] K.Harikumar, M. Seetharama Bhat, " Path generation and integrated guidance and control of a micro air vehicle", *IEEE MSC Conference* , August 28-30, pp. 1024-1029, India, 2013.
[23] H. Jiankun, C. Bohn, H.R. Wu, " Systematic H_∞ weighting function selection and its application to the real-time control of a vertical take-off aircraft", *Control engineering Practice*, Vol.8, pp.241-252, 2000. CrossRef
[24] U. Mackenroth, "*Robust control systems, theory and case studies*", Springer , pp. 350, 2004. CrossRef